Advanced Composite Materials
Publication details, including instructions for authors and subscription information:
http://www.tandfonline.com/loi/tacm20

Oxidation Behaviors and Mechanisms of C/Si-C-N with a Mullite Interlayer

Guofeng Lu [a], Shengru Qiao [b], Chengyu Zhang [c] & Gengsheng Jiao [d]

[a] National Key Laboratory of Thermostructure Composite Materials, Northwestern Polytechnical University, Xi'an 710072, China; Department of Chemistry and Chemical Engineering, Weinan Teachers University, Weinan 714000, China;, Email: luguof.student@sina.com

[b] National Key Laboratory of Thermostructure Composite Materials, Northwestern Polytechnical University, Xi'an 710072, China

[c] National Key Laboratory of Thermostructure Composite Materials, Northwestern Polytechnical University, Xi'an 710072, China

[d] Department of Chemistry and Chemical Engineering, Weinan Teachers University, Weinan 714000, China

Version of record first published: 02 Apr 2012.

To cite this article: Guofeng Lu , Shengru Qiao , Chengyu Zhang & Gengsheng Jiao (2011): Oxidation Behaviors and Mechanisms of C/Si-C-N with a Mullite Interlayer, Advanced Composite Materials, 20:2, 179-195

To link to this article: http://dx.doi.org/10.1163/092430410X539280

VSP

Advanced Composite Materials 20 (2011) 179–195

ADVANCED COMPOSITE MATERIALS
brill.nl/acm

Oxidation Behaviors and Mechanisms of C/Si–C–N with a Mullite Interlayer

Guofeng Lu [a,b,*], **Shengru Qiao** [a], **Chengyu Zhang** [a] **and Gengsheng Jiao** [b]

[a] National Key Laboratory of Thermostructure Composite Materials, Northwestern Polytechnical University, Xi'an 710072, China

[b] Department of Chemistry and Chemical Engineering, Weinan Teachers University, Weinan 714000, China

Received 22 January 2010; accepted 10 August 2010

Abstract

Carbon fiber reinforced Si–C–N matrix composite with a mullite interlayer (C/Mullite/Si–C–N) was fabricated *via* CVI and PIP process. The oxidation behaviors of C/Mullite/Si–C–N were investigated in air by comparison with that of C/PyC/Si–C–N using thermogravimetry and SEM technique. The results indicate that the weight loss of the C/Mullite/Si–C–N increases with the increase of the temperature below 800°C, decreases in the range of 800–1000°C, and increases again above 1000°C. The increase of the weight loss below 800°C results from the increase of the oxidation temperature. The closure of the matrix microcracks at 800–1000°C leads to the decrease of the weight loss, and the reopening of microcracks results in the increase above 1000°C. The oxidation resistance of C/Mullite/Si–C–N was improved greatly as compared to C/PyC/Si–C–N within the temperature range from 600°C to 1200°C. The mullite interphase changes the oxidation mode of C/Si–C–N and leads to the non-uniform oxidation of carbon fibers in the composite. At 600°C, the oxidation curve of C/Mullite/Si–C–N shows obvious non-linearity, which mainly results from the non-uniform oxidation of carbon fibers.

Keywords

Oxidation, mullite interlayer, C/Si–C–N, composites, carbon fiber

1. Introduction

The oxidation protection of carbon fiber reinforced ceramic matrix composites (CFCMCs) has attracted increasing interest in recent years. There are many ways to improve the oxidation resistance of the CFCMCs, including designing a non-oxidizable coating [1–4], adding additives into the matrix [5–7], and so

* To whom correspondence should be addressed. E-mail: luguof.student@sina.com
Edited by KSCM

DOI:10.1163/092430410X539280

on. Choosing a suitable interphase for the composites was an important method. S. Labruquère and his co-workers [8] had selected BC, Si–B–C and SiC as the interphase to improve the oxidation resistance of CFCMCs. Their results proved that the suitable interphase could protect the carbon fiber from oxidation and enhance the oxidation resistance of the composite.

Mullite is a promising candidate material for the oxidation protection, owing to its low thermal conductivity, excellent creep resistance, good chemical stability and low oxygen diffusivity [9]. So far, the mullite had been used as an interlayer of C/Si–C–N composite and can greatly improve the oxidation resistance of composites [10]; but the oxidation behaviors and mechanisms of C/Si–C–N with a mullite interlayer are still unclear.

In the present work, the carbon fiber reinforced Si–C–N matrix composite with a mullite interphase (C/Mullite/Si–C–N) was fabricated. The oxidation behaviors of the C/Mullite/Si–C–N were investigated, and the oxidation mechanism was analyzed by the comparison between the oxidation behaviors of C/Mullite/Si–C–N and that of C/Si–C–N with a pyrocarbon interlayer (C/PyC/Si–C–N).

2. Experimental

2.1. Sample Preparation

The needle-pricked long fiber felt with a density of 0.6 g/cm^3, fabricated with T300 carbon fibers, was used as preform. In order to investigate the oxidation mechanisms of composites, two kinds of materials, C/Mullite/Si–C–N and C/Si–C–N with a pyrocarbon interlayer (C/PyC/Si–C–N), were fabricated. Mullite interphase was prepared *via* a polymer impregnation and pyrolysis (PIP) process using the mixture of aluminium *sec*-butoxide ($A1(OBu)_3$) and tetraethoxysilicate (TEOS) as the starting materials. The details about the preparation of the mullite interphase were described elsewhere [10, 11]. The carbon interlayer was deposited at 900°C for 2 h using propene as precursor. The average thicknesses of both mullite interlayer and PyC interlayer are about 500 nm. Si–C–N matrix of C/Mullite/Si–C–N and C/PyC/Si–C–N was prepared through a chemical vapor infiltration (CVI) process at 900°C for 10 h using hexamethyldisilazane (HMDS) as single precursor. HMDS was bubbled at room temperature by Ar carrier gas and the mixed gases were introduced into the chamber at a flow rate of 5 cm^3/min through a stainless-steel tube. The chamber pressure during deposition was maintained at atmospheric pressure. An argon atmosphere was used during the preparation of the SiCN matrix. The density and porosity of the as-prepared C/Si–C–N composites were ∼1.82 g/cm^3 and about 8–10%, respectively, measured by Archimedes method.

2.2. Oxidation Tests

Specimens were machined from the as-prepared C/Si–C–N composites for the oxidation test. The required specimen size was 3.5 mm × 3.5 mm × 20 mm. Oxidation

tests were carried out in a tubular furnace. Firstly, the furnace was heated to the preset temperature for 20–30 min, and then the samples were put into the center of the furnace. At the given time, the samples were weighed by a photoelectric analytical balance with a sensitivity of ±0.0001 g (Model AG135, Mettler Toledo).

3. Results and Discussion

3.1. Microstructure of C/Si–C–N

Figures 1 and 2 show the microstructure of C/Mullite/Si–C–N. Owing to the mismatch of the thermal expansion coefficient between the fiber and the matrix, some microcracks exist in the C/Mullite/Si–C–N. In addition, restrained by the preparation method of the preform and CVI process, there are a lot of residual pores in C/Mullite/Si–C–N. The microcracks and the residual pores will act as the channels for diffusion of oxiding gases during oxidation.

Figure 3 shows the mullite interlayer of the composite. Both matrix/mullite interlayer bond and mullite interlayer/fiber bond are tight.

3.2. Weight Loss as a Function of Time

Figure 4 shows the isothermal oxidation curves of the C/Mullite/Si–C–N at different temperatures. The mass loss of the composite oxidized at 600°C and 700°C increases with the duration of the time. The isothermal oxidation curves of the composite oxidized at the temperature from 800°C to 1200°C can be divided into two parts: the weight of samples rapidly decreases with the oxidation time before the

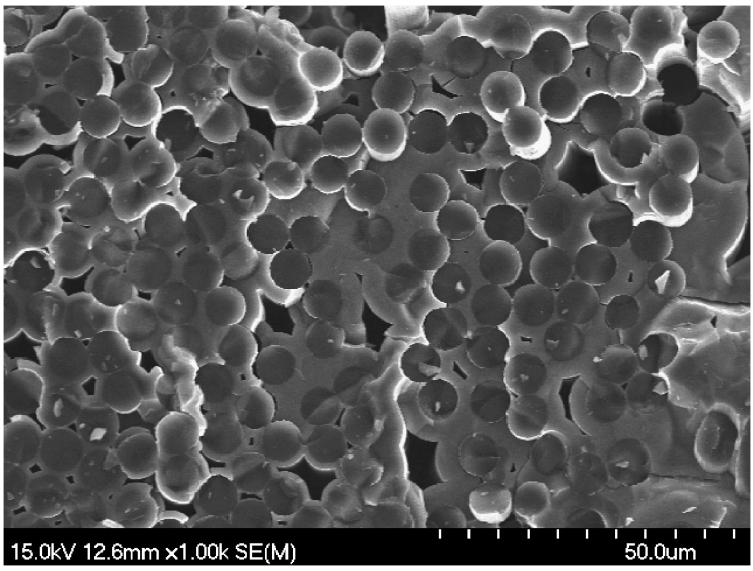

Figure 1. SEM fractograph of C/Mullite/Si–C–N.

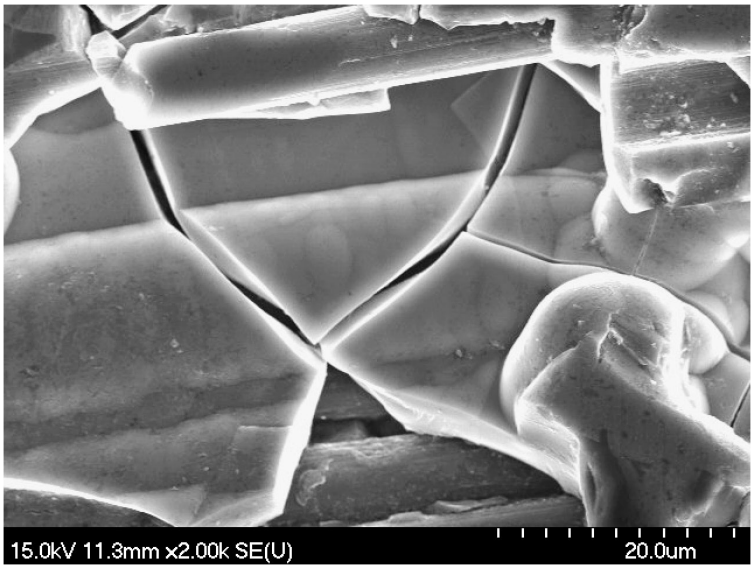

Figure 2. Microcracks in the composite.

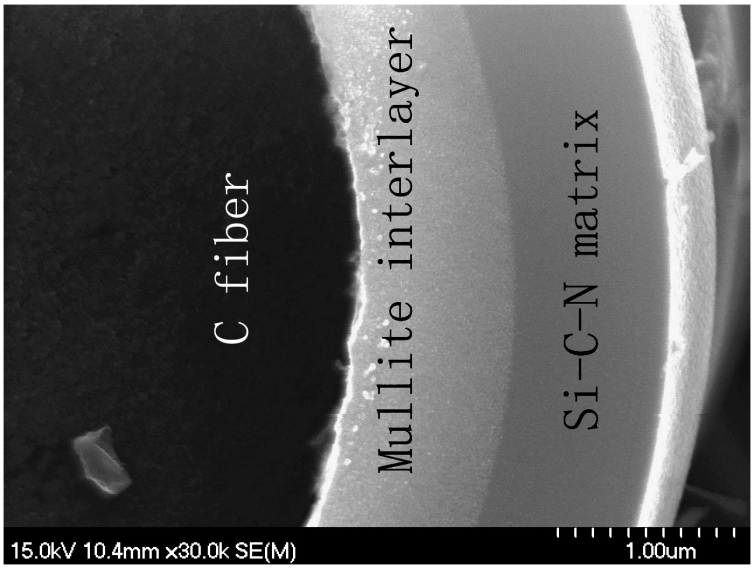

Figure 3. SEM image of the mullite interlayer.

weight loss reaches the maximum value; and increases slowly after the weight loss reaches the maximum value.

Figure 5 is an SEM fractograph of C/Mullite/Si–C–N before and after oxidation at different temperature. With the increase of the time and temperature, the corrosion on the carbon fiber became more and more serious. 6.5 hours' oxidation at

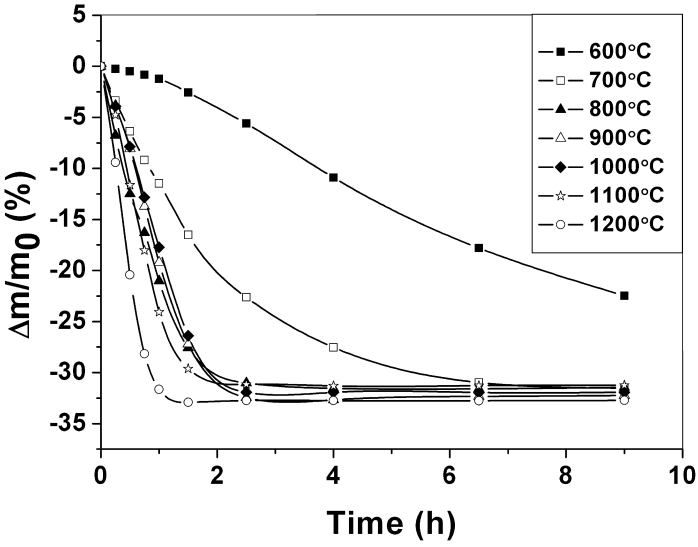

Figure 4. Isothermal oxidation curve of C/Si–C–N.

800°C has resulted in the disappearance of carbon fiber in the composite (Fig. 5(d)), and after oxidation at 800°C for 2.5 h, carbon fibers cannot even be seen on fracture of the composite (Fig. 5(e)), which indicates that the carbon fibers have been completely consumed.

There are some oxygen-containing gases in air such as oxygen itself, water vapor, carbon dioxide, etc. These gases will react with the carbon fiber and Si–C–N matrix of the composite in a hot environment. The escape of CO_2 and/or CO formed during the oxidation of the carbon will result in the weight loss of the composite [12], while the oxidation of the Si–C–N leads to the weight gain because oxygen atoms substitute for the carbon atom and nitrogen atom in Si–C–N [13]. At 600°C and 700°C, the Si–C–N hardly is oxidized, so the weight loss of the composite can be considered as the result of the oxidation of carbon fiber. As the oxidation of carbon fiber continued, the weight loss of the composite increased. At the temperature from 800°C to 1200°C, only slight oxidation of Si–C–N has occurred and the weight gain resulting from oxidation of Si–C–N is very small because of the excellent oxidation resistance of Si–C–N, so the mass change of the composite can be considered as the result of the oxidation of carbon fiber, approximately. Therefore, the weight loss of the composite increased with time. When the weight loss reaches the maximum value, the carbon fibers of the composites have been completely oxidized and only the mullite interphase and Si–C–N matrix remained (Fig. 5(e)). As the oxidation of the Si–C–N matrix is continued, the mass of the composite increased slowly.

3.3. Weight Loss as a Function of Temperature

Figure 6 shows the weight change with the oxidation temperature. It can be seen that the weight loss of the C/Mullite/Si–C–N increases with the increase of the

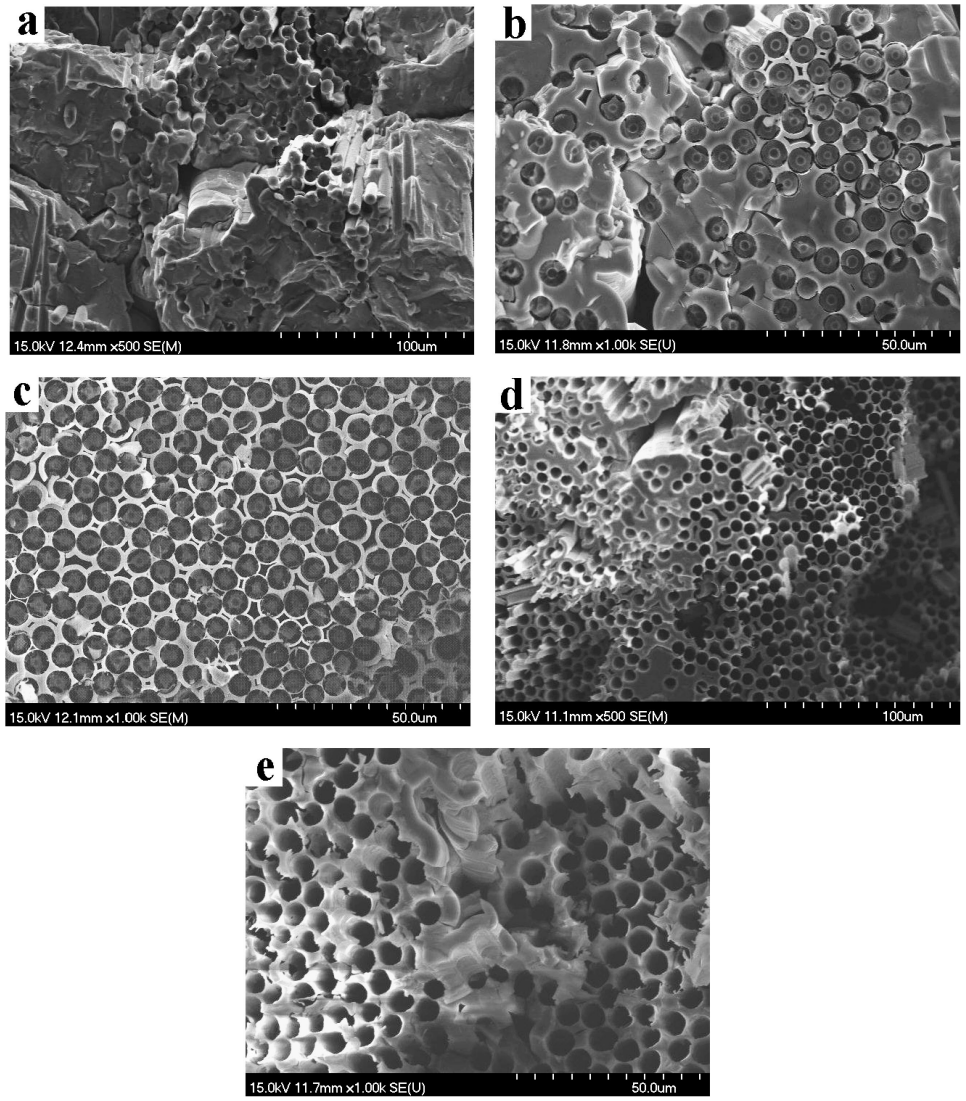

Figure 5. SEM fractograph of C/Mullite/Si–C–N before and after oxidation at different temperature: (a) before oxidation; (b) oxidation at 600°C for 6.5 h; (c) oxidation at 600°C for 9 h; (d) oxidation at 700°C for 6.5 h; (e) oxidation at 800°C for 2.5 h.

temperature below 800°C, decreases in the range of 800–1000°C, and increases again above 1000°C, which is different from that of C/SiC and C/C. These results indicate that the oxidation resistance of the composite is improved in the range from 800°C to 1000°C.

The above relationship between weight changes of the C/Mullite/Si–C–N and oxidation temperature might be related with the oxidation kinetics of the carbon fiber and evolution of the cracks in C/Mullite/Si–C–N with temperature. When the

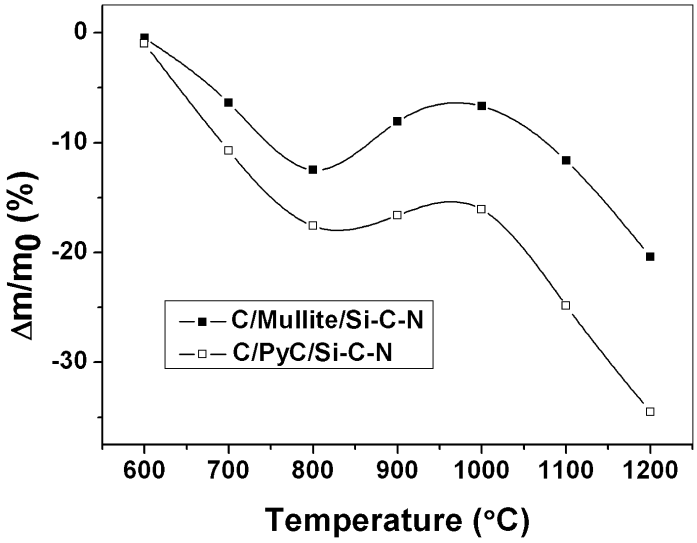

Figure 6. Relative mass variations as a function of temperature for C/Si–C–N.

samples without coating were exposed to the hot air, the carbon fibers and matrix on the surface of composite would be firstly oxidized. With the oxidation of carbon fiber, a great many ducts opening to the surface of the sample were formed. These ducts will permit the diffusion of the oxidizing gases Also, the oxidizing gases can diffuse into the sample through the microcracks and the residual pores in the composite shown in Figs 1 and 2. When the temperature is below 800°C, the oxidation of carbon fiber is controlled by the velocity of a chemical reaction between the carbon fiber and the oxidizing gases. The reaction velocity will increase with the temperature, so the weight loss of the composite follows. If the temperature is above 800°C, the oxidation of carbon fiber is controlled by the diffusion of the oxide gases [14, 15]. The rate of diffusion is directly proportional to the diffusion area, so the variation in the diffusion channels of the oxide gases will have an immediate influence on the oxidation rate of the carbon fiber. During the oxidation, although the channels formed by oxidation of carbon fiber and the residual pores in the composite do not change with temperature, the width of matrix cracks in composite will decrease with the increase of temperature, which will decrease the rate of diffusion. Despite the fact that the diffusion rate will increase with the increase of the temperature, which cannot offset the influence of the clogging of the matrix cracks, the diffusion quantity of the oxide gases within unit time decreases. Previous results [16, 17] show that the matrix cracks of composites will clog below the processing temperature of the matrix. However, it can be seen from Fig. 6 that the weight loss of C/Mullite/Si–C–N still continues the trend of decline above the processing temperature, which is 900°C, until 1000°C. This result indicates that the matrix cracks of C/Mullite/Si–C–N maybe clog at about 1000°C, that is, 100°C higher than the deposition temperature of Si–C–N. The increase of the

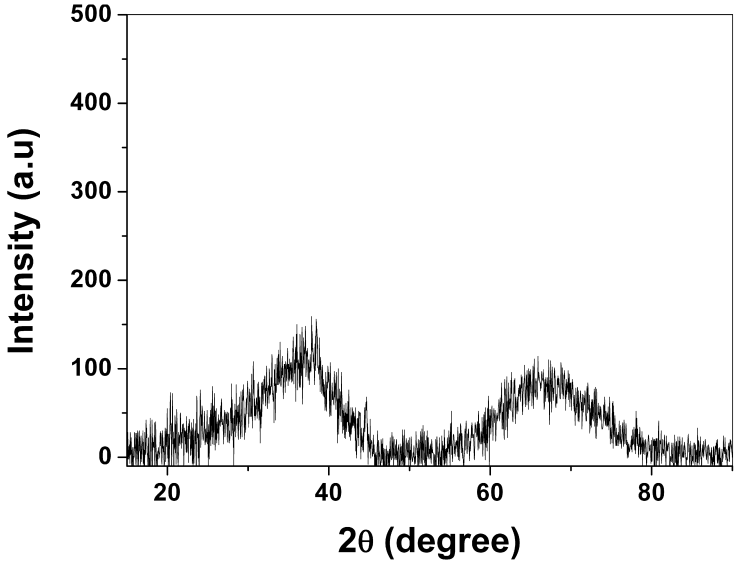

Figure 7. XRD pattern of Si–C–N matrix.

clogging temperature possibly results from the amorphism of the Si–C–N matrix (Fig. 7). It is well known that an amorphous substance will be gradually crystallized at higher temperature. The theoretical density of crystalline Si–C–N is about 3.08 g/cm^3, while the amorphous Si–C–N fabricated in this work only has a density of 2.23 g/cm^3, measured by Archimedes method. So an increase in density must accompany the crystallization of Si–C–N matrix. These densification processes result in the volume shrinkage, which will decrease the expansion increment of the matrix, and consequently make the matrix cracks unable to clog below the processing temperature, so that the clogging temperature is increased. When the temperature is above 1000°C, the shrinkage resulting from the densification processes speeds up and the rate of shrinkage becomes higher than the rate of thermal expansion; therefore, the closed cracks will reopen, which can be confirmed by Fig. 8, and the diffusion of oxidizing gases increases. In addition, the diffusion of oxide gases also increases with the increase of temperature. So the weight loss of composite rapidly increases with the increase of temperature.

3.4. Influence of Mullite Interphase on the Oxidation Behaviors of C/Si–C–N

From Fig. 6, it can be seen that the weight loss of C/Mullite/Si–C–N is obviously less than that of C/PyC/Si–C–N within the whole temperature range, which confirms the higher oxidation resistance of C/Mullite/Si–C–N. Figure 9 shows the isothermal oxidation curves of the C/Mullite/Si–C–N and C/PyC/Si–C–N at 600°C. It can be seen that the oxidation rate of C/Mullite/Si–C–N first increases and then decreases with time. The oxidation curve of C/Mullite/Si–C–N shows obvious nonlinearity compared with that of C/PyC/Si–C–N.

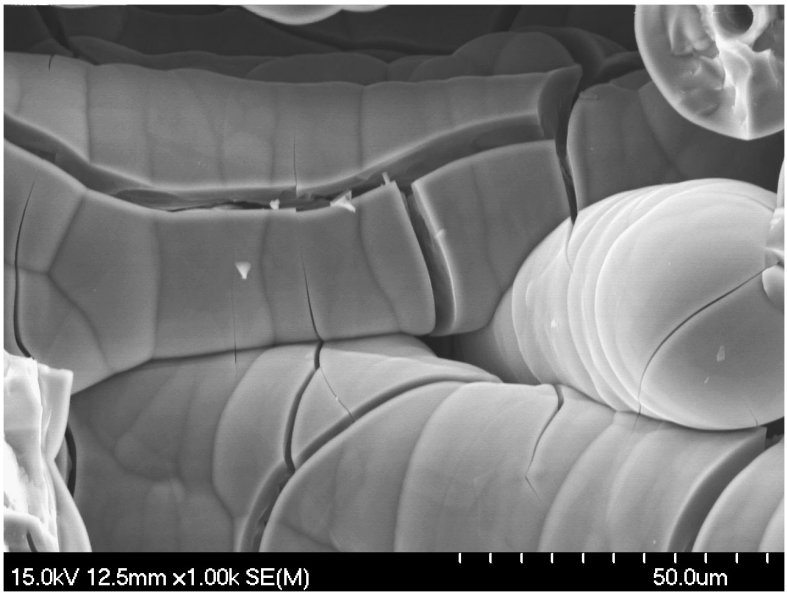

Figure 8. SEM fractograph of C/Mullite/Si–C–N after oxidation at 1100°C for 4 h.

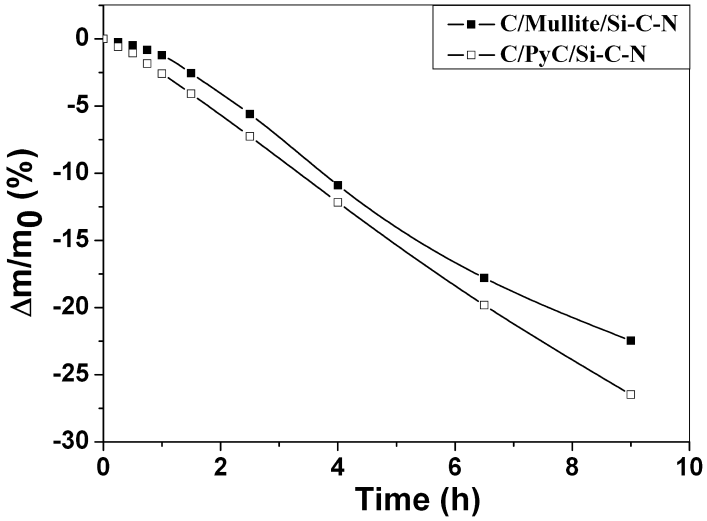

Figure 9. Comparison between isothermal oxidation curve of C/Mullite/Si–C–N and that of C/PyC/Si–C–N at 600°C.

Not only the higher oxidation resistance but also the non-linear oxidation curve of C/Mullite/Si–C–N is related to the mullite interlayer. The matrix cracks in composites result from the thermal stress (σ_m) in the matrix. The σ_m will decide the width and the density of cracks. The σ_m can be calculated through the following

Table 1.
The calculated value of σ_m and the physical parameters of C/Mullite/Si–C–N and C/PyC/Si–C–N

	C/Mullite/Si–C–N	C/PyC/Si–C–N
T_P (°C)	900	900
T_R (°C)	25	25
α_m (K^{-1})	1.9×10^{-6}	1.9×10^{-6}
α_{int} (K^{-1})	4.4×10^{-6} [9]	4.7×10^{-6} [18]
α_f (K^{-1})	1×10^{-6}	1×10^{-6} [19]
E_m (GPa)	190	190 [20]
E_{int} (GPa)	167 [21]	10 [22]
E_f (GPa)	230	230 [23]
V_m (%)	48	47
V_{int} (%)	10	10
V_f (%)	34	34
σ_m (MPa)	25.6	66.5

equation:

$$\begin{aligned}\sigma_m &= E_m \Delta T(\alpha_m - \alpha_{com}) \\ &= E_m(T_P - T_R)\left(\alpha_m - \frac{\alpha_m E_m V_m + \alpha_i E_i V_i + \alpha_f E_f V_f}{E_m V_m + E_i V_i + E_f V_f}\right),\end{aligned} \tag{1}$$

where T_P is the preparation temperature, T_R is room temperature, the α, E and V are the coefficient of thermal expansion (CTE), Young's modulus and volume fraction respectively. The subscripts m, i and f represent the matrix, interlayer and carbon fiber, respectively. The calculated value of σ_m and the physical parameters of the individual components in C/Mullite/Si–C–N and C/PyC/Si–C–N are listed in Table 1. It can be seen that σ_m of C/Mullite/Si–C–N, which is 25.6 MPa, is very much lower than that of C/PyC/Si–C–N, which is 66.5 MPa. Therefore, the microcrack density in C/Mullite/Si–C–N would be obviously lower than that of C/PyC/Si–C–N, which is confirmed by Fig. 10. The lower density of matrix cracks suggests less active points on the carbon fiber, which may be the reason why C/Mullite/Si–C–N has higher oxidation resistance. In addition, the tight interfacial bond of C/Mullite/Si–C–N will be another contribution to the enhancement of the oxidation resistance. Figure 11 is an SEM image of C/PyC/Si–C–N, it can be seen that the gaps can be observed at the interfaces both between the fiber and the interphase and between the matrix and the interphase. According to Figs 11 and 3, it can be seen that the interfacial bonding of C/Mullite/Si–C–N is tighter than that of C/PyC/Si–C–N. It is more difficult for the oxidizing gases to diffuse along the tightly bonded interface than along the weak interface. So, it is more difficult to oxidize the carbon fiber in C/Mullite/Si–C–N compared to that in C/PyC/Si–C–N, so that this property was beneficial to the improvement of oxidation resistance of C/Mullite/Si–C–N.

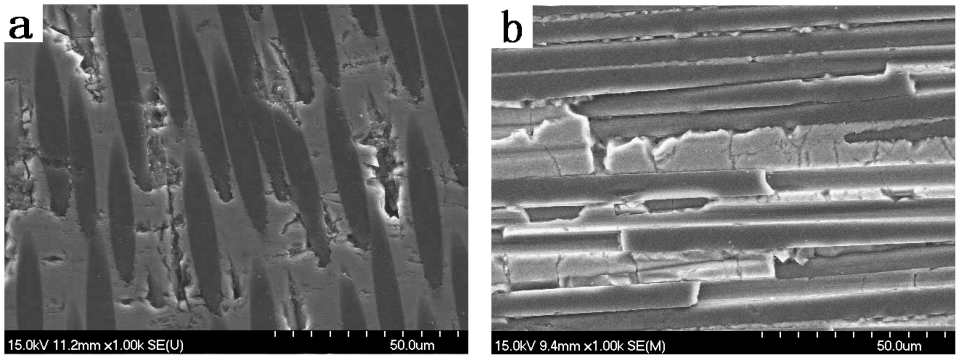

Figure 10. SEM micrograph of as-prepared C/Si–C–N composites: (a) C/Mullite/Si–C–N; (b) C/PyC/Si–C–N.

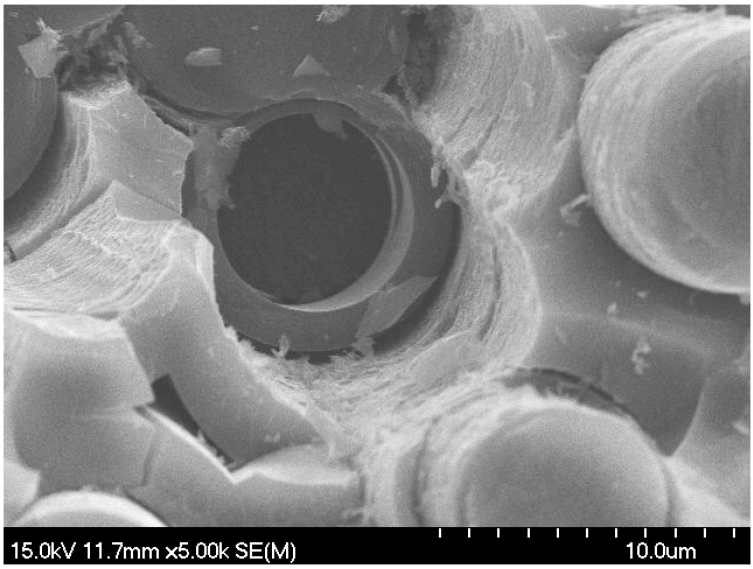

Figure 11. SEM fractograph of C/PyC/Si–C–N.

The strong interfacial bond also greatly influences the oxidation characteristics of C/Mullite/Si–C–N. The strong interfacial bond does not easily allow the oxide gases to diffuse along the interface, so the oxidation of carbon fiber will be limited around the crossing point of cracks and carbon fiber (Fig. 12). Thus, some corrosion pits are formed on the carbon fiber (Fig. 13), and each corrosion pit will extend along the direction vertical to the oxidation surface with the increase of the oxidation time, which leads to the non-uniform oxidation of carbon fibers (Fig. 14). The oxidation process can be schematically described by Fig. 15. For C/PyC/Si–C–N, the weak bond will allow the oxide gases to diffuse through the gaps between the fiber and the interphase and between the matrix and the interphase, so the oxidation almost simultaneously occurs on the entire fiber surface (Fig. 16), characterized by the

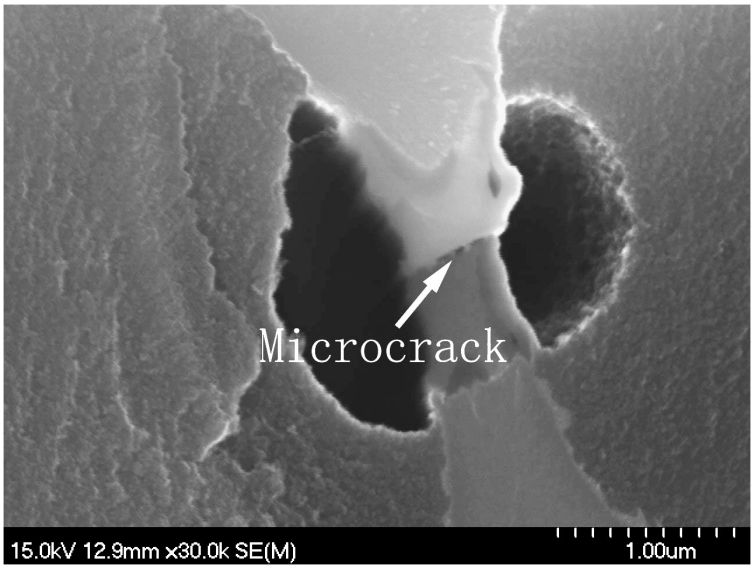

Figure 12. The corrosion pits in the neighborhood of a microcrack.

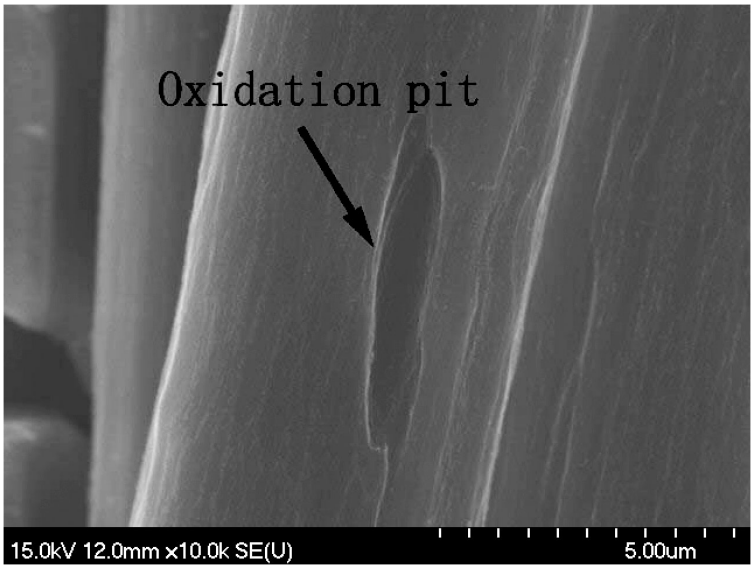

Figure 13. SEM image of the corrosion pits on carbon fiber.

mode of uniform oxidation. This kind of oxidation mode will just result in the decrease in fiber diameter (Fig. 17) and does not form the obvious corrosion pits on the carbon fibers. Because the oxidation rate is directly related with the oxidation area on the carbon fiber [13], the change of oxidation area with time will lead to the variation of the oxidation rate. In the case of non-uniform oxidation, given that the

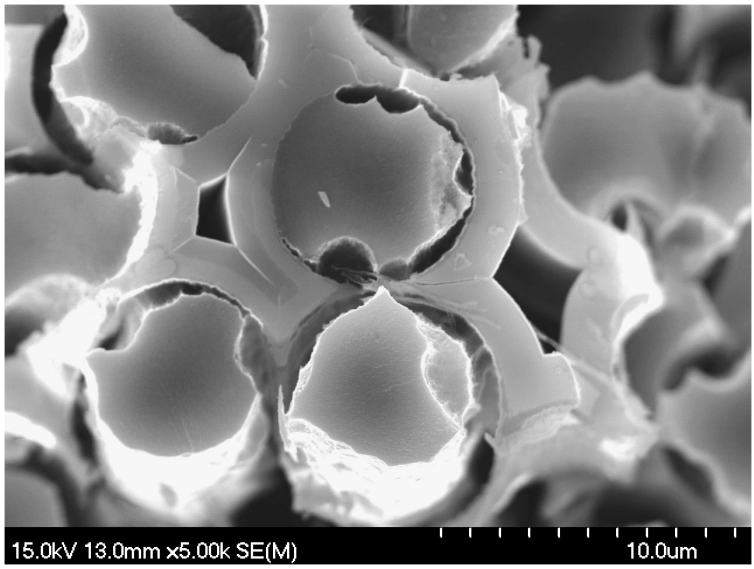

Figure 14. SEM fractograph of C/Mullite/Si–C–N after oxidation at 600°C for 6.5 h.

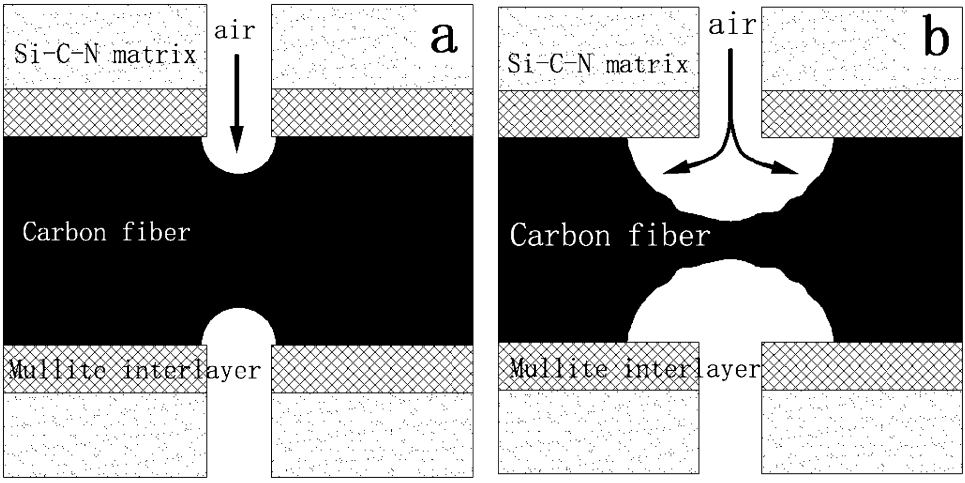

Figure 15. Schematic diagram for oxidation process of C/Mullite/Si–C–N: (a) oxidation at an early stage; (b) after oxidation for a long time.

oxidation face is round with a corrosion point as center, the morphological model of composite during oxidation can be described by Fig. 18. Based on this model, the oxidation area (S) can be expressed as:

$$S = 2\sum_{i=1}^{\rho V} l_i \cdot \arccos\left(\frac{vt}{2R}\right) vt, \tag{2}$$

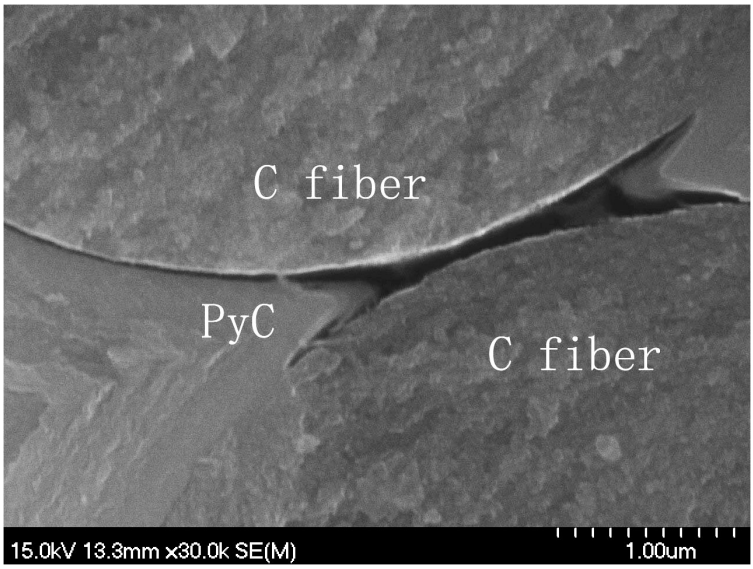

Figure 16. SEM fractograph of C/PyC/Si–C–N after oxidation at 600°C for 0.5 h.

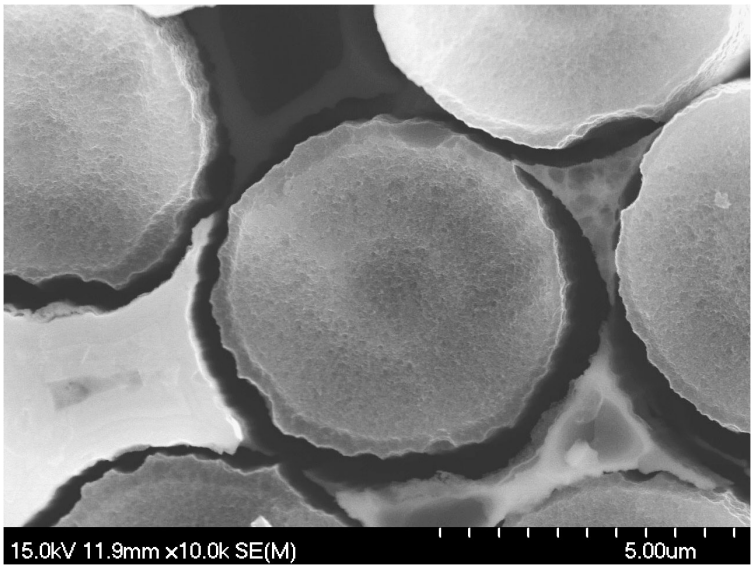

Figure 17. SEM fractograph of C/PyC/Si–C–N after oxidation at 600°C for 2.5 h.

where ρ is the crack density of composite, V is the volume of a sample for oxidation test, l is the length of a crack, R is the radius of carbon fibers, v is the reaction rate, and t is oxidation time. From equation (2), it can be seen that oxidation area firstly increases and then decreases with time, so the oxidation rate also follows this pattern. From the above discussion, we can think that the non-uniform oxidation of

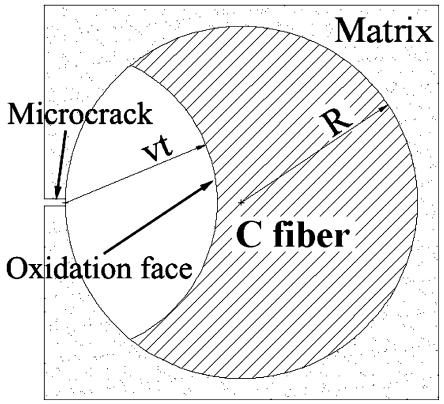

Figure 18. Morphological model of the carbon fiber in composite.

the carbon fibers leads to the non-linearity of the oxidation curve of C/Mullite/Si–C–N. For C/PyC/Si–C–N, before the carbon interlayer was completely consumed, the oxidation area hardly changes. So the weight loss changes linearly with time. It must be pointed out that the non-linearity of the oxidation curve of C/Mullite/Si–C–N only appears below 800°C. At higher temperature, the oxidation of carbon fiber is controlled by the diffusion of the oxide gases, and the oxidation of the carbon fibers in the composite does not occur at the same time, so the oxidation curve would be linear.

4. Conclusions

When the composites were oxidized at the temperature range from 600°C to 1200°C, all the samples show the decrease in weight with the oxidation time before the weight loss reaches the maximum value and a slight increase after the weight loss reaches the maximum value. The weight loss of the C/Mullite/Si–C–N linearly increases with the increase of the temperature below 800°C, decreases in the range of 800–1000°C, and increases again above 1000°C. The increase of the weight loss below 800°C results from the increase of the oxidation temperature. The closure of the matrix microcracks at 800–1000°C leads to the decrease of the weight loss and the reopening of microcracks results in the increase above 1000°C. The Mullite interlayer can improve the oxidation resistance of C/Si–C–N. The low density of cracks and the tight interfacial bond in C/Mullite/Si–C–N contribute to the enhancement of the oxidation resistance. The mullite interlayer also changes the oxidation mode of C/Si–C–N and leads to the non-uniform oxidation of carbon fibers in the composite. At 600°C, the oxidation curve of C/Mullite/Si–C–N shows obvious non-linearity. The non-uniform oxidation of carbon fibers is the key reason for the non-linearity of the oxidation curve of C/Mullite/Si–C–N.

Acknowledgements

This research has been supported by the National Natural Science Foundation of China (Program No. 50772089), Scientific research project of Shaanxi Provincial Department of Education (Program No. 09JK425) and the Foundation of Weinan Teachers University (Program No. 10YKZ052).

References

1. C. Argirusis, T. Damjanović and G. Borchardt, Yttrium silicate coating system for oxidation protection of C/C–Si–SiC composites: electrophoretic deposition and oxygen self-diffusion measurements, *J. Eur. Ceram. Soc.* **27**, 1303–1306 (2007).
2. Z. Q. Yan, X. Xiong, P. Xiao, F. Chen, H. B. Zhang and B. Y. Huang, A multilayer coating of dense SiC alternated with porous Si–Mo for the oxidation protection of carbon/carbon silicon carbide composites, *Carbon* **46**, 149–153 (2008).
3. Z. Q. Yan, X. Xiong, P. Xiao, F. Chen, H. B. Zhang and B. Y. Huang, Si–Mo–SiO_2 oxidation protective coatings prepared by slurry painting for C/C–SiC composites, *Surf. Coat. Technol.* **202**, 4734–4740 (2008).
4. J. Li, R. Y. Luo, C. Lin, Y. H. Bi and Q. Xiang, Oxidation resistance of a gradient self-healing coating for carbon/carbon composites, *Carbon* **45**, 2471–2478 (2007).
5. G. H. Zhou, S. W. Wang, X. X. Huang and J. K. Guo, Improvement of oxidation resistance of unidirectional C_f/SiO_2 composites by the addition of SiCp, *Ceram. Intl* **34**, 331–335 (2008).
6. C. Q. Tong, L. F. Cheng, X. W. Yin, L. T. Zhang and Y. D. Xu, Oxidation behavior of 2D C/SiC composite modified by SiB_4 particles in inter-bundle pores, *Compos. Sci. Technol.* **68**, 602–607 (2008).
7. R. Y. Luo, Z. Yang and L. F. Li, Effect of additives on mechanical properties of oxidation resistant carbon/carbon composite fabricated by rapid CVD method, *Carbon* **38**, 2109–2115 (2000).
8. S. Labruquère, H. Blanchard, R. Pailler and R. Naslain, Enhancement of the oxidation resistance of interfacial area in C/C composites. Part II: Oxidation resistance of B–C, Si–B–C and Si–C coated carbon preforms densified with carbon, *J. Eur. Ceram. Soc.* **22**, 1011–1021 (2002).
9. T. Damjanovic, C. Argirusis, G. Borchardt, H. Leipner, R. Herbig, G. Tomandl and R. Weiss, Oxidation protection of C/C–SiC composites by an electrophoretically deposited mullite precursor, *J. Eur. Ceram. Soc.* **25**, 577–587 (2005).
10. G. F. Lu, S. R. Qiao, C. Y. Zhang, J. T. Hou, D. C. Jia and Y. B. Zhang, Oxidation protection of C/Si–C–N composite by a mullite interphase, *Composites Part A* **39**, 1467–1470 (2008).
11. G. F. Lu, S. R. Qiao, J. T. Hou and M. F. Gong, Mullite interlayer of C/Si–C–N composites fabricated by PIP, *Mater. Sci. Forum* **575–578**, 881–885 (2008).
12. X. W. Yin, L. F. Cheng, L. T. Zhang and Y. D. Xu, Oxidation behaviors of C/SiC in the oxidizing environments containing water vapor, *Mater. Sci. Engng A* **348**, 47–53 (2003).
13. D. Bahloul, P. Goursat and A. Lavedrine, Influence of microstructural changes on the oxidation resistance of silicon carbonitrides derived from a polyvinylsilazane, *J. Eur. Ceram. Soc.* **11**, 63–68 (1993).
14. W. M. Guo, H. N. Xiao, E. Yasuda and Y. Cheng, Oxidation kinetics and mechanisms of a 2D-C/C composite, *Carbon* **44**, 3269–3276 (2006).
15. F. Lamouroux, X. Bourrat and R. Naslain, Structure/oxidation behavior relationship in the carbonaceous constituents of 2D-C/PyC/SiC composites, *Carbon* **31**, 1273–1288 (1993).

16. F. Lamouroux, G. Camus and J. Thébault, Kinetics and mechanisms of oxidation of 2D woven C/SiC composites: I, Experimental approach, *J. Amer. Ceram. Soc.* **77**, 2049–2057 (1994).
17. L. F. Cheng, Y. D. Xu, L. T. Zhang and X. W. Yin, Oxidation behavior of three dimensional C/SiC composites in air and combustion gas environments, *Carbon* **38**, 2103–2108 (2000).
18. R. I. Baxter, R. D. Rawlings, N. Iwashita and Y. Sawada, Effect of chemical vapor infiltration on erosion and thermal properties of porous carbon/carbon composite thermal insulation, *Carbon* **38**, 441–449 (2000).
19. J. X. Zhao, K. H. Ding and J. X. Wei, Research on thermophysical properties and anti-thermal-vibration properties of C/C composites, *Acta Mater. Compos. Sinica* **4**, 45–50 (1987).
20. P. Jedrzejowski, J. Cizek, A. Amassian, J. E. Klemberg-Sapieha, J. Vlcek and L. Martinua, Mechanical and optical properties of hard SiCN coatings prepared by PECVD, *Thin Solid Films* **447–448**, 201–207 (2004).
21. H. Schneider, J. Schreuer and B. Hildmann, Structure and properties of mullite — a review, *J. Eur. Ceram. Soc.* **28**, 329–344 (2008).
22. J. F. Wu, S. Bai and H. M. Cheng, Influence of heat treatment on microstructure and mechanical properties of isotropic pyrolytic carbon, *New Carbon Mater.* **21**, 225–230 (2006).
23. G. Camus, L. Guillaumat and S. Baste, Development of damage in a 2D woven C/SiC composite under mechanical loading: I. Mechanical characterization, *Compos. Sci. Technol.* **56**, 1363–1372 (1996).